Numerical study of grating-assisted optical diffraction tomography

Patrick C. Chaumet, Kamal Belkebir, and Anne Sentenac

Institut Fresnel (UMR 6133), Université d'Aix-Marseille I & III, Avenue Escadrille Normandie-Niemen,
F-13397 Marseille Cedex 20, France

We study the resolution of an optical diffraction tomography system in which the objects are either in an homogeneous background or deposited onto a glass prism, a prism surmounted by a thin metallic film or a prism surmounted by a metallic film covered by a periodically nanostructured dielectric layer. For all these configurations, we present an inversion procedure that yields the map of the relative permittivity of the objects from their diffracted far field. When multiple scattering can be neglected, we show that the homogeneous, prism, and metallic film configurations yield a resolution about $\lambda/4$ while the grating substrate yields a resolution better than $\lambda/10$. When Born approximation fails, we point out that it is possible to neglect the coupling between the object and the substrate and account solely for the multiple scattering within the objects to obtain a satisfactory reconstruction. Last, we present the robustness of our inversion procedure to noise.

PACS number(s): 42.30.Wb, 42.25.Fx

I. INTRODUCTION

Developing optical imaging systems with a power of resolution below 100 nm without bringing a probe in the vicinity of the sample stirs considerable interest. The applications are numerous especially in the nanotechnology [1] and biological domains [2]. The usual barrier to be broken is the well known Rayleigh criterion that states that two radiating dipoles will be distinguishable on the image of their far-field intensity if their interdistance is greater than $1.22\lambda/2 \approx 0.6\lambda$, where λ is the wavelength of radiation. This criterion applies to classical microscopes [3] but is expected to be beaten by a factor of 2 in an optical diffraction tomography experiment [4,5]. In this very recent technique, the sample is illuminated along different directions of incidence and the amplitude and phase of the far field are detected for many angles of observations. The image, i.e., the map of relative permittivity, is then numerically synthesized from the diffracted far-field data.

To ameliorate the resolution of far-field optical imaging systems, several means have been proposed. The most famous consists of diminishing the illuminating wavelength by immersing the samples in a liquid with high refractive index n. More recently, it has been proposed to illuminate the sample with evanescent waves through a prism while collecting the diffracted field in the far field. This option has led to total internal reflection microscopes (TIRM) [6] and total internal reflection tomography (TIRT) [7,8]. These techniques are adapted to surface imaging, like near-field optical microscopes, but they do not require one to scan a probe above the object and they provide an instantaneous widefield image of the surface. Their power of resolution is better than the spatial frequency of the incident field, i.e., the index of refraction of the prism, is high. Unfortunately, in optics, the highest refractive index available for the prism function in TIRM or TIRT is close to two. Other imaging configurations take advantage of the properties of surface plasmons. The sample is deposited on a thin metallic film illuminated under Kretschmann configuration. The plasmon excitation permits one to enhance the field at the surface of the sub-

strate and thus to increase the sensitivity to small permittivity variations localized at the interface [9]. Plasmon-assisted microscopes have been shown to distinguish two dots whose center interdistance is roughly 140 nm for a free-space wavelength of 500 nm [10]. Recently, it has been proposed to deposit the sample onto an optimized grating in order to increase the spatial frequencies of the illuminating field beyond that reachable with a prism or a metallic film alone. A resolution of $\lambda/10$ has been obtained with simulated data in a grating-assisted optical diffraction tomography (ODT) [11], in which the sample is deposited on a periodically nanostructured substrate and the permittivity map is reconstructed numerically from the diffracted far-field. In another context, a resolution about $\lambda/4$ has been observed experimentally in a grating-assisted microscopy [12]. The goal of this paper is to compare the performances of the grating-assisted ODT to that of the free-space, prism-assisted, and plasmon-assisted ODT.

In Sec. II we recall the principles of ODT and we present the different experimental configurations. In Sec. III, we sketch the numerical technique that is used to simulate the experiment and we detail the inversion algorithms that synthesize the map of relative permittivity of the sample from the simulated diffracted far-field data. Last, in Sec. IV, we compare the power of resolution of the different configurations and we point out the role of multiple scattering in the inversion procedures [13].

II. BASIC ANALYSIS OF THE RESOLUTION IN OPTICAL DIFFRACTION TOMOGRAPHY

In an optical diffraction tomography experiment (see Fig. 1), the sample is illuminated successively by different incident plane waves with wave vectors $\mathbf{k}^{\mathrm{inc}}$ and the complex amplitude $\mathbf{e}(\mathbf{k}, \mathbf{k}^{\mathrm{inc}})$ of its diffracted plane wave with wave vector $\mathbf{k}$ is measured for various angles of observation. The map of the relative permittivity of the sample is then reconstructed from the diffracted far-field data $\mathbf{e}(\mathbf{k}, \mathbf{k}^{\mathrm{inc}})$.

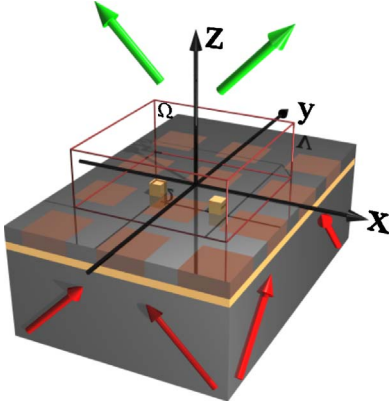We will first consider a configuration in which the sample

FIG. 1. (Color online) Geometry of the imaging system. The objects are deposited on a nanostructured substrate and successively illuminated from below by height plane waves. The incident angle with respect to Oz is always $80°$ while the incident angle with respect to Ox varies with a step of $45°$. The far field is detected above the substrate along 80 directions equally spaced within a cone of half-angle $70°$.

is in vacuum (free space). Under single scattering, one can show that the diffracted far-field $\mathbf{e}(\mathbf{k},\mathbf{k}^{\mathrm{inc}})$ is proportional to the spatial Fourier transform of the relative permittivity of the sample, $\hat{\varepsilon}(\mathbf{k}^{\mathrm{inc}}-\mathbf{k})$ [14]. Hence, performing a simple 3D inverse Fourier transform on the measured data permits one to reconstruct the image of the sample [4]. In an ideal far-field imaging system, with all possible angles of incidence and detection, the Fourier transform of the relative permittivity is known in a sphere of radius $4\pi/\lambda$. By performing a three-dimensional inverse Fourier transform of this low-pass binary optical transfer function, one gets the point spread function of the imaging system. The expected resolution of this complete imaging system, given by the width at mid-height of the point spread function, is about $\lambda/3$ in the three dimensions.

In this work, we consider an optical diffraction tomography in transmission in which the sample is illuminated from below, $k_z^{\mathrm{inc}}=\mathbf{k}^{\mathrm{inc}}\cdot\hat{z}>0$, and the scattered far field is measured above the sample, $k_z=\mathbf{k}\cdot\hat{z}>0$. Note that, throughout the paper, an $\exp(-i\omega t)$ dependence, with $2\pi/\lambda=\omega/c=k_0$, is assumed and omitted. In this asymmetric configuration, the transverse resolution in the (x,y) plane remains close to 0.3λ while that in the axial direction is about 0.6λ [4,5,13]. In the following, we will focus solely on the transverse resolution as we are mainly interested in surface imaging.

We now study an experimental configuration in which the sample is deposited onto a prism and illuminated under total internal reflection. In this case, the field scattered by the sample cannot be linked easily to the 3D Fourier transform of the relative permittivity. Yet, relatively simple calculations using the Green tensor of the stratified medium and assuming Born approximation show that the amplitude of the field scattering in the $\mathbf{k}=(\mathbf{k}_{\parallel},k_z)$ direction of an object illuminated by an incident plane wave with wave vector $\mathbf{k}^{\mathrm{inc}}=(\mathbf{k}_{\parallel}^{\mathrm{inc}},k_z^{\mathrm{inc}})$ is linked to the 2D Fourier transform of the relative permittivity via [7],

$$\mathbf{e}(\mathbf{k},\mathbf{k}^{\mathrm{inc}}) = \int \mathbf{F}(k_z,k_z^{\mathrm{inc}},z) \times [\varepsilon(\mathbf{r})-1]e^{-i(\mathbf{k}_{\parallel}-\mathbf{k}_{\parallel}^{\mathrm{inc}})\cdot\mathbf{r}_{\parallel}}d\mathbf{r}_{\parallel}dz, \tag{1}$$

where $\mathbf{F}$ is a known vectorial function that does not depend on the object placed on the prism. From Eq. (1) it is seen that, if the axial dimension of the sample is small compared to the wavelength, and if its relative permittivity is invariant in the z direction, $\varepsilon(\mathbf{r})=\varepsilon(\mathbf{r}_{\parallel})$, then the far-field amplitude $\mathbf{e}(\mathbf{k},\mathbf{k}^{\mathrm{inc}})$ yields the 2D-Fourier amplitude of the permittivity $\hat{\varepsilon}(\mathbf{k}_{\parallel}^{\mathrm{inc}}-\mathbf{k}_{\parallel})$. Hence, a transverse resolution of $0.6\lambda/(n+1)$ can be expected at best.

To generate an incident field with higher transverse spatial frequency than that obtainable with a prism, it is necessary to overcome the bounds (namely, 2) imposed by the available refraction indices of lossless materials in the optical domain. Hence, we will consider a configuration in which the sample is deposited on a substrate that is periodically nanostructured along the $\hat{\mathbf{x}}$ and $\hat{\mathbf{y}}$ direction, with period d [11]. Indeed, if one illuminates a two-dimensional grating by a plane wave with wave vector $\mathbf{k}^{\mathrm{inc}}$, the field above the grating can be written as a Rayleigh series [15],

$$\mathbf{E}^{\mathrm{inc}}(\mathbf{k}_{\parallel}^{\mathrm{inc}},\mathbf{r}_{\parallel},z) = \sum_{\mathbf{K}\in W} \mathbf{E_K}(\mathbf{k}_{\parallel}^{\mathrm{inc}})e^{i[(\mathbf{K}+\mathbf{k}_{\parallel}^{\mathrm{inc}})\cdot\mathbf{r}_{\parallel}+ik_z^{\mathbf{K}}z]}, \tag{2}$$

where W denotes the reciprocal space of the periodic structure, $W=\{\mathbf{K}=n(2\pi/d)\hat{\mathbf{x}}+m(2\pi/d)\hat{\mathbf{y}}$ with $(n,m)\in\mathbb{Z}^2\}$ and $k_z^{\mathbf{K}}=[k_0^2-|\mathbf{K}+\mathbf{k}_{\parallel}^{\mathrm{inc}}|^2]^{1/2}$, with the imaginary part of k_z positive. From Eq. (2) it is easily seen that, provided that $\mathbf{E_K}$ does not decay too quickly with increasing $\mathbf{K}$, the field that will illuminate the objects present high spatial frequencies. If sole one order, denoted by $\mathbf{E_{K_c}}$, is predominant in Eq. (2), the grating acts as a prism with an effective index $n_c=|\mathbf{k}_{\parallel}^{\mathrm{inc}}+\mathbf{K}_c|/k_0$. In this case, the simple relationship, Eq. (1), between the diffracted far field and the Fourier amplitude of the relative permittivity can be used to estimate the resolution of the system. The latter will be all the better than n_c is large. This diffracting property can be obtained with grating couplers, which are composed of a multilayer stack surmounted by a small periodic corrugation. The role of the corrugation is to convert the incident wave into a mode of the multilayer, either a guided wave [16] or a surface plasmon [15]. To generate a mode with high spatial frequencies, we have considered a thin metallic film that supports long-range and short-range surface plasmons. The wave vectors $\mathbf{k}_p$ of the short-range plasmons are all the larger than the film thickness is small [17,18]. These modes can be excited by a free-space incident plane wave if there exists one vector of the reciprocal space $\mathbf{K}_c$ of the grating such that the phase matching condition [15],

$$\mathbf{k}_p \approx \mathbf{k}_{\parallel}^{\mathrm{inc}} + \mathbf{K}_c \tag{3}$$

is satisfied. The excitation of the mode corresponds to a resonance phenomenon that increases the amplitude of the field corresponding to the $\mathbf{K}_c$ order in Eq. (2). If the mode is a guided wave or a long-range plasmon, the field amplitude $\mathbf{E_{K_c}}$ can be several orders of magnitude larger than all the other terms in Eq. (2). Unfortunately, contrary to long-range

plasmons or guided waves, short-range plasmons whose wave vector modulus is much larger than the free-space wave number k_0 present high losses. Hence, they are difficult to excite even with an optimized periodic perturbation. In all the structures we have studied, the field amplitude $\mathbf{E}_{\mathbf{K}_c}$, which is the signature of the plasmon excitation, turned out to be comparable to the specular transmitted amplitude $\mathbf{E}_0$. The presence of these two orders create an interference pattern at the surface of the grating so that the field intensity repartition is strongly inhomogeneous. To avoid the formation of blind and bright spots, *i.e.*, regions where the illuminating field is always weak or strong, we have checked that the average of the field intensity over all the incidences be roughly homogeneous within one period of the grating. This is obtained if the periodic modulation is weak. The chosen grating is the same as that described in Ref. [11]. It consists of a substrate made of a 7 nm silver film, embedded in a glass prism, and a 7 nm layer of SiO$_2$ with n_{SiO_2}=1.5. This last layer is etched with square holes that are filled with Ta$_2$O$_5$, with $n_{\mathrm{Ta}_2\mathrm{O}_5}$=2.1. The square period d of the bidimensional square grating is 100 nm while the side of the holes is 67 nm and the free-space wavelength of illumination is λ=500 nm. The short-range plasmon that can be excited with this structure, taking n_{silver}=0.12+2.91i, has a wave number close to $6k_0$, much larger than that obtained with a classic plasmon-assisted sensor under Kretschmann configuration. In the grating configuration, the relationship between the far-field data and the relative permittivity is not as simple as that given in Eq. (1) since the object is illuminated simultaneously by several plane waves, as seen in Eq. (2). Hence, the scattered field will not be linked to only one Fourier amplitude of the relative permittivity but to many of them. The issue is then to verify that the inversion algorithms will be able to unravel these different coefficients.

We now describe the numerical tools that have enabled us to simulate the tomography experiment in its various configurations.

III. THEORY

A. Forward scattering problem

We compute the field scattered by the sample in our tomography experiment by a volume integral equation technique known as the coupled dipole method (CDM). Initially, this method has been developed to compute the scattering by objects in an homogeneous space [19], then, a few years ago it has been applied to the scattering by objects in the presence of a multilayer system [20,21], and very recently it has addressed the difficult issue of the scattering by aperiodic objects in the presence of a grating [22]. The principle of this technique is to consider the objects as a perturbation of a reference medium, the latter being an homogeneous medium in the free-space configuration, the multilayer in the stratified configuration, or the periodically nanostructured substrate in the grating configuration. We introduce the field susceptibility tensor $\overset{\leftrightarrow}{\mathbf{G}}$ such that $\overset{\leftrightarrow}{\mathbf{G}}(\mathbf{r},\mathbf{r}')\mathbf{p}(\mathbf{r}')$ is the electric field at $\mathbf{r}$ radiated by a dipole $\mathbf{p}(\mathbf{r}')$ placed at $\mathbf{r}'$ in the reference medium and $\mathbf{E}^{\mathrm{inc}}$ is the reference field that exists in the absence

of the object [23]. We now discretize the object into a cubic array of K polarizable subunits centered about $\mathbf{r}_i$, i=1,…,K, whose size d is small enough compared to the spatial variations of the electromagnetic field for the dipole approximation to apply. We call $\varepsilon(\mathbf{r}_i)$ the relative permittivity of the subunit centered about $\mathbf{r}_i$. The electric local field at each subunit position is derived from the self-consistent equation

$$\mathbf{E}(\mathbf{r}_i) = \mathbf{E}^{\mathrm{inc}}(\mathbf{r}_i) + \sum_{k=1}^{K} \overset{\leftrightarrow}{\mathbf{G}}(\mathbf{r}_i,\mathbf{r}_k)\alpha(\mathbf{r}_k)\mathbf{E}(\mathbf{r}_k), \qquad (4)$$

where $\alpha(\mathbf{r}_k)$ is the polarizability of subunit located at the position $\mathbf{r}_k$ as follows:

$$\alpha(\mathbf{r}_k) = \frac{3d^3}{4\pi}\frac{\varepsilon(\mathbf{r}_k)-1}{\varepsilon(\mathbf{r}_k)+2}. \qquad (5)$$

In Eq. (5) we neglect the radiative reaction term; for more details about this term and the recent evolution of the CDM, see Refs. [24,25]. Equation (4) is a linear system whose size is $3K \times 3K$. Once the local field $\mathbf{E}(\mathbf{r}_i)$ is known at each $\mathbf{r}_i$, for i=1,…,K, the electric field can be computed everywhere outside the object through the equation

$$\mathbf{E}(\mathbf{r}) = \mathbf{E}^{\mathrm{inc}}(\mathbf{r}) + \sum_{k=1}^{K} \overset{\leftrightarrow}{\mathbf{G}}(\mathbf{r},\mathbf{r}_k)\alpha(\mathbf{r}_k)\mathbf{E}(\mathbf{r}_k). \qquad (6)$$

From Eqs. (4) and (6), it appears that the key point of the CDM is to calculate the field susceptibility tensor for the various reference geometries. Its expression is given, in the case of a homogeneous space, in Ref. [26], and in the case of a stratified medium, in Refs. [20,27]. An evaluation of the field susceptibility tensor, when the reference problem is a grating, has been recently proposed in Ref. [22]. Note that there is a small difference in the geometry of the present study and that of Ref. [22] due to the presence of a metallic layer between the grating and the substrate. To take into account this layer one needs only to change the Fresnel coefficient of the field susceptibility of the substrate according to Ref. [28] and use this new tensor inside Ref. [22].

Finally, in all the chosen configurations, the field diffracted by the object under study at M observation points for L different incidence angle can be written symbolically as

$$\mathbf{E}_l^d = \overset{=}{\mathbf{B}}\alpha\mathbf{E}_l, \qquad (7)$$

where l=1,…,L, and $\overset{=}{\mathbf{B}}$ is a matrix of size $(3M \times 3K)$. The matrix $\overset{=}{\mathbf{B}}$ contains the field susceptibility tensors $\overset{\leftrightarrow}{\mathbf{G}}(\mathbf{r}_k,\mathbf{r}_j)$, where $\mathbf{r}_j$ denotes a point in the discretized object, j=1,…,K, while $\mathbf{r}_k$ is an observation point k=1,…,M. $\overset{=}{\mathbf{B}}$ does not depend on the angle of incidence. $\alpha\mathbf{E}_l$ is a vector of size $3K$ which represents, for each angle of incidence, the dipole moment induced at each point of discretization of the object. With this approach, we are able to simulate "rigorously" a tomography experiment. We now describe briefly the technique used to reconstruct the map of relative permittivity of the unknown object from the measures of its diffracted far field.

B. Inverse scattering problem

We assume that the unknown three-dimensional object is entirely confined in a bounded box $\Omega \subset \mathbb{R}^3$ (test domain or an investigating domain) and illuminated successively by $l = 1, \dots, L$ electromagnetic excitation $\mathbf{E}^{\text{inc}}_{l=1,\dots,L}$ (see Fig. 1). For each excitation l, the scattered field $\mathbf{f}^d_l$ is measured on a surface Γ at M points and located outside the investigating domain Ω.

The inverse scattering problem is stated as finding the relative permittivity distribution ε inside the investigating area Ω such that the associated scattered field matches the measured field $\mathbf{f}^d_{l=1,\dots,L}$. In the present paper, we choose an iterative approach, close to that described in Refs. [8,13,29] to solve this nonlinear and ill-posed inverse scattering problem. We mesh Ω into Q regular subunits and we call α_n the complex Q vector of the reconstructed polarizability of each subunit at the nth iteration. Starting from an initial guess, one adjusts α_n gradually by minimizing a cost functional involving the measured scattered-field data. The sequence $\{\alpha_n\}$ is built up according to the following recursive relation:

$$\alpha_n = \alpha_{n-1} + a_n d_n, \tag{8}$$

where the updated polarizability α_n is deduced from the previous one α_{n-1} by adding a correction $a_n d_n$. This correction is composed of two terms: a scalar weight a_n and an updating direction d_n. Once the updating direction d_n is found, and this will be specified later in the paper, the scalar weight a_n is determined by minimizing the cost functional $\mathcal{F}_n(\alpha_n)$ involving the residual error $\mathbf{h}_{l,n}$ on the scattered field computed from observation equation [Eq. (7)]

$$\mathbf{h}_{l,n} = \mathbf{f}^d_l - \overset{\leftrightarrow}{\mathbf{B}} \alpha_n \mathbf{E}_{l,n}, \tag{9}$$

with $\mathbf{E}_{l,n}$ being the total electric field that would be present in Ω if the polarizability distribution was α_{n-1}. The field $\mathbf{E}_{l,n}$, is obtained by solving the dense linear system described by Eq. (4) with the polarizability taken equal to $\{\alpha_{n-1}\}$. This calculation can be very time consuming, especially in the grating-substrate configuration, for which the field susceptibility tensor is not invariant by translation. When the objects are much smaller than the wavelength, the renormalized Born approximation [8], i.e., $\mathbf{E}_{l,n} = \mathbf{E}^{\text{inc}}_{l,n}$, can be successfully used. Note that the Born approximation consists of assimilating the macroscopic field inside the object to the incident field while the renormalized Born approximation amounts to assimilating the local field inside the object to the incident field. The latter is more accurate than the former. This assumption greatly diminishes the time of computation but it does not account for the multiple scattering phenomena. When the renormalized Born approximation is not valid, we propose to solve Eq. (4) by replacing the field susceptibility tensor $\overset{\leftrightarrow}{\mathbf{G}}$ of the reference grating geometry by that of the homogeneous space or that of the stratified medium. This approximation permits one to greatly simplify the resolution of the linear system, Eq. (4), since the tensor operator becomes a toeplitz matrix [30,31]. This approximation amounts to neglecting part of the interaction between the object and the substrate while retaining multiple scattering within the object. Note that whatever the level of approximation chosen for solving

the near-field equation, Eq. (4), the field susceptibilities tensors that appear in the far-field equation, Eq. (9), as well as the incident field, are always computed exactly. Indeed, it has been shown [8] that an approximation on the far-field operator has more impact on the reconstructions than an approximation on the near-field operator. The calculation of the far-field operator is quite easy since, invoking the reciprocity theorem, it is equivalent to the calculation of the field illuminating the object [22].

The cost functional $\mathcal{F}_n(\alpha_n)$ mentioned above that is minimized at each iteration step reads as

$$\mathcal{F}_n(\alpha_n) = \frac{\sum_{l=1}^{L} \|\mathbf{h}_{l,n}\|^2_\Gamma}{\sum_{l=1}^{L} \|\mathbf{f}_l\|^2_\Gamma} = W_\Gamma \sum_{l=1}^{L} \|\mathbf{h}_{l,n}\|^2_\Gamma, \tag{10}$$

where the subscript Γ is included in the norm $\|\cdot\|$ and later the inner product $\langle\cdot|\cdot\rangle$ in L^2 to indicate the domain of integration.

Substituting the expression of the polarizability α_n derived from Eq. (8) in Eq. (10) leads to a polynomial expression with respect to the scalar coefficient a_n. Thus the minimization of the cost functional $\mathcal{F}_n(\alpha_n)$ is reduced to a minimization of a simple cost function $\mathcal{F}_n(a_n)$,

$$\mathcal{F}_n(a_n) = W_\Gamma \sum_{l=1}^{L} (\|\mathbf{h}_{l,n-1}\|^2_\Gamma + |a_n|^2 \|\overset{\leftrightarrow}{\mathbf{B}} d_n \mathbf{E}_{l,n-1}\|^2_\Gamma$$
$$- 2a_n \operatorname{Re}\langle \mathbf{h}_{l,n-1}|\overset{\leftrightarrow}{\mathbf{B}} d_n \mathbf{E}_{l,n-1}\rangle_\Gamma). \tag{11}$$

In this case, the unique minimum of $\mathcal{F}_n(a_n)$ is reached for

$$a_n = \frac{\sum_{l=1}^{L} \langle \overset{\leftrightarrow}{\mathbf{B}} d_n \mathbf{E}_{l,n-1}|\mathbf{h}_{l,n-1}\rangle_\Gamma}{\sum_{l=1}^{L} \|\overset{\leftrightarrow}{\mathbf{B}} d_n \mathbf{E}_{l,n-1}\|^2_\Gamma}. \tag{12}$$

As updating direction d_n, the authors take the Polak-Ribiére conjugate gradient direction

$$d_n = g_{n;\alpha} + \gamma_n d_{n-1}, \tag{13}$$

where g_n is the gradient of the cost functional $\mathcal{F}_n$ with respect to the polarizability assuming that the total fields $\mathbf{E}_l$ do not change.

$$g_{n;\alpha} = -W_\Gamma \sum_{l=1}^{L} \mathbf{E}^*_{l,n-1} \cdot \overset{\leftrightarrow}{\mathbf{B}}^\dagger \mathbf{h}_{l,n-1}, \tag{14}$$

in which $\mathbf{u}^*$ denotes the complex conjugate of $\mathbf{u}$ and $\overline{\overline{\mathbf{B}}}^\dagger$ represents the transpose complex conjugate matrix of the matrix $\overline{\overline{\mathbf{B}}}$.

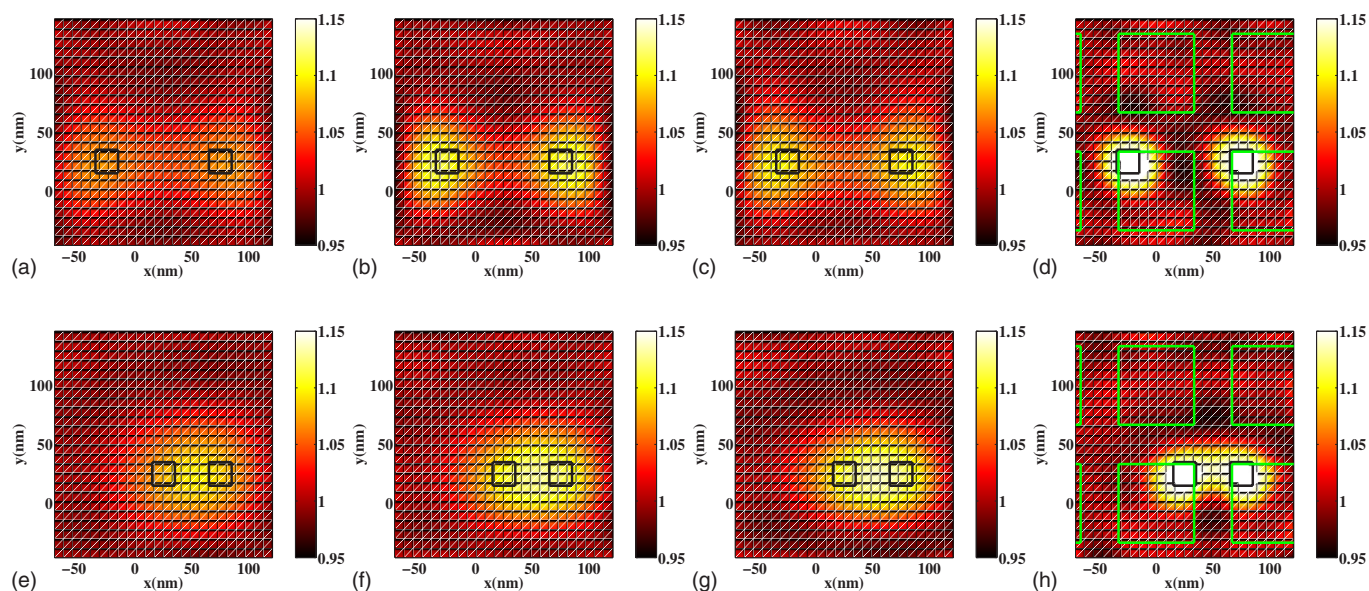The scalar coefficient γ_n is defined as in Polak-Ribière conjugate-gradient method [32]

FIG. 2. Map at $z=12$ nm of the relative permittivity given by our inversion scheme. The investigation domain is a $200 \times 200 \times 40$ nm^3 box placed on the grating. The objects are two cubes of glass with side $\lambda/30$. For (a), (b), (c), and (d), the center interdistance of the cubes is $\lambda/5$ while for (e), (f), (g), and (h) it is $\lambda/10$. In (a) and (e) the objects are in homogeneous space, in (b) and (f) the objects are on a glass prism, in (c) and (g) the objects are on a glass prism coated with a 7-nm-thin metallic film, and in (d) and (h) the objects are on a grating made of Ta$_2$O$_5$, pads embedded in a 7 nm layer of SiO$_2$, and deposited on a 7 nm silver film onto the glass prism. The squares indicates the position of the Ta$_2$O$_5$ pads (see Fig. 1).

$$\gamma_n = \frac{\langle g_{n;\alpha} | g_{n;\alpha} - g_{n-1;\alpha} \rangle_\Gamma}{\| g_{n-1;\alpha} \|_\Gamma^2}. \quad (15)$$

The initial guess of the iterative algorithm α_0 is estimated with a back-propagation procedure [8]. Note that we did not assume any hypothesis on the polarizability of the subunits. Hence, the reconstruction procedures yield a complex relative permittivity although we consider lossless objects. Last, we point out that, in all our simulations, the meshing used for the direct problem is different from that used for the inversion.

IV. SOME EXAMPLES OF RECONSTRUCTION FROM SIMULATED DATA SET

In all the numerical experiments, the incident beam is coming from the glass substrate and makes an angle of 80° with respect to the z axis. This angle has been chosen so that Eq. (3) with $\mathbf{K}_c = \frac{2\pi}{d}\hat{\mathbf{x}}$ is roughly satisfied in the grating configuration. To excite the short-range plasmon, the incident polarization is chosen in the incident plane. We have used height different illuminations by rotating the incident plane of 45° about the z axis. The scattered field is detected in the superstrate for 80 angles of observation within a cone of half-angle 70°.

A. Two dipoles: Study of the resolution

To point out the resolution of the different configurations, we first consider an object made of two cubes of glass with side $\lambda/20$, small enough so that they can be considered as dipoles. In Fig. 2, the distance between the cubes center is taken equal to $\lambda/5=100$ nm and $\lambda/10=50$ nm. In this paragraph, the inversion is performed under the renormalized Born approximation so that solely the far-field susceptibility tensors of the different configurations are necessary to minimize Eq. (10). We plot the real part of the reconstructed map of relative permittivity (the retrieved imaginary part is always lower than 0.05), for the homogeneous space configuration, Figs. 2(a) and 2(e), the prism configuration, Figs. 2(b) and 2(f), the prism covered by the thin metallic layer, Figs. 2(c) and 2(g), and the prism covered by the metallic layer and the grating, Figs. 2(d) and 2(h). As expected, we observe that when the dipoles interdistance is $\lambda/5$, the two cubes are hardly distinguished in the homogeneous space configuration, while they are clearly seen with the prism, the multilayer, and the grating substrate. We observe that the presence of the metallic layer does not ameliorate the image as compared to that of the prism. Hence, even though the short-range plasmons of the metallic film are excited by the isolated objects, they modify marginally the scattering behavior of the cubes. In particular, they do not generate a multiple scattering phenomenon, which could have been used to ameliorate the resolution with an adequate nonlinear inversion algorithm [13,33]. On the contrary, a dramatic improvement is obtained with the grating configuration in which the short-range plasmon is strongly excited by the periodic substrate. This result is confirmed on the reconstructed images of the two cubes when their center interdistance is taken equal to $\lambda/10$. In this case, solely the grating-configuration enables one to distinguish the two cubes. Since this configuration is not invariant by translation, we have checked that the two cubes could be distinguished whatever their relative position with respect to the periodic substrate. This numerical experiment shows that, with a linear inver-
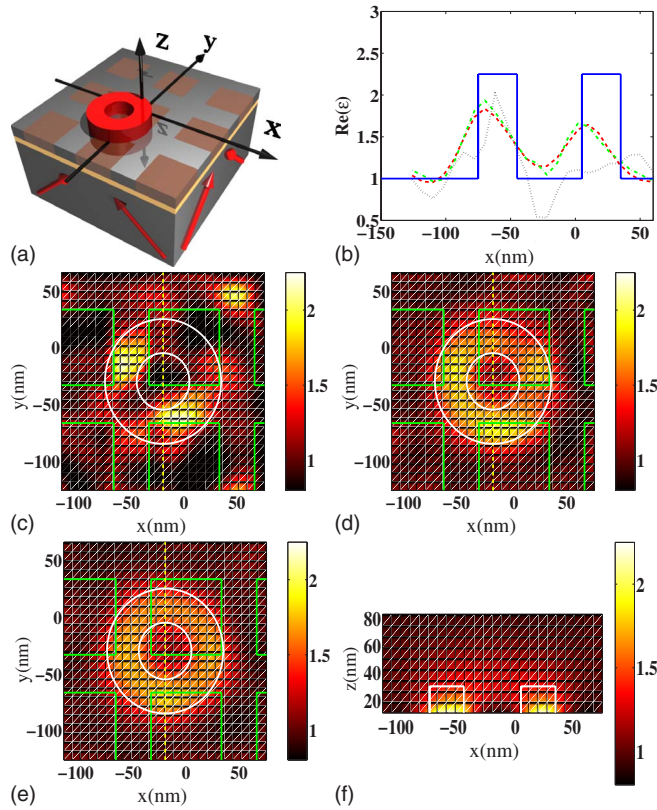
(a)

(b)

(c)

(d)

(e)

(f)

FIG. 3. (Color online) (a) Geometry of the imaging configuration. The object is a glass rectangular tore with an inner radius of 25 nm and an outer radius of 50 nm. The height of the object is 30 nm. We plot the map of the relative permittivity at $z=12$ nm for three different reconstruction procedures. (c) Renormalized Born approximation. (d) Nonlinear inversion. The field susceptibility used in Eq. (4) is that of vacuum. (e) Same as (d) but the field susceptibility is that of the substrate with the top nanostructured layer replaced by an homogeneous film of SiO$_2$. (f) Same as (e) but the map of relative permittivity is plotted in the (x,z) plane at $y=-30$ nm. (b) Value of the relative permittivity obtained along the dashed vertical line in (c) (dotted line), (d) (dashed line), and (e) (dash-dotted line)

sion algorithm, a resolution about $\lambda/10$ can be expected with the grating configuration. We now turn to a more complex problem in which the test object is larger and supports multiple scattering.

B. Tore: Role of multiple scattering

In this paragraph, we consider solely the grating configuration. We have taken a tore-shaped object made of glass, of inner diameter $\lambda/10$, and an outer one $\lambda/5$ with height 0.06λ, as depicted in Fig. 3(a). This object has been chosen to point out the influence of the nonhomogeneity of the substrate. In Fig. 3(c) we plot the reconstructed map of relative permittivity obtained with the renormalized Born approximation. The result clearly shows that this approximation is not valid in this case. Note that this approximation holds when the object is small with respect to the investigating wavelength. In the grating configuration, the object is probed with a plasmon with a spatial frequency of $6k_0$, hence single scat-
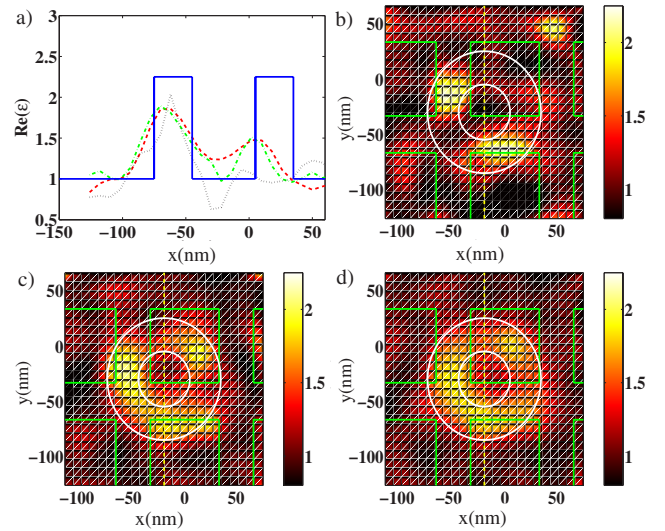

a)

b)

c)

d)

FIG. 4. (Color online) Same as Figs. 3(b)–3(e) but the diffracted field is corrupted with noise (Fig. 3).

tering approximation may be accurate when the object is in the homogeneous space and totally wrong when the object is deposited on the grating substrate. To account for part of the multiple scattering, we first calculate at each iteration the field $\mathbf{E}_{l,n}$ inside Ω by solving Eq. (4) with the field-susceptibility tensor of the homogeneous reference problem. The reconstructed relative permittivity obtained with this approximation is shown in Fig. 3(d). The image is clearly improved; the tore is now clearly visible, i.e., the hole of the tore is perfectly retrieved [see profile Fig. 3(b)], and the relative permittivity found is close to 2.25. In Fig. 3(e), we use the field susceptibility tensor of the multilayer for solving Eq. (4). This more accurate estimation of the field susceptibility yields an amelioration of the image inasmuch as the tore appears to be more homogeneous. Yet, the value of the relative permittivity is slightly underestimated by our inversion scheme. This problem could be solved with an adequate regularization procedure, by introducing some *a priori* information on the sample. Hence, accounting for multiple scattering within the object and neglecting the coupling with the substrate reconstruction is an interesting way for improving the image without dramatically increasing the computation time. In Fig. 3(e) and more clearly in Fig. 3(d), the "errors" in the estimation of the relative permittivity are localized about the edges of the grating. In Fig. 3(f), we observe that the image resolution, indicated by the ability to distinguish the hole within the ring, diminishes as one moves away from the interface. This is not surprising since the resolution is obtained thanks to the evanescent waves whose weight decreases quickly far from the grating.

In Fig. 4, we check the robustness of our calculation to noise. We corrupt the diffracted field $\mathbf{f}_l^d$, with a complex uniform noise defined as follows:

$$\mathbf{f}_l^d = \mathrm{Re}(\mathbf{E}_l^d)(1+u\,\eta) + i\,\mathrm{Im}(\mathbf{E}_l^d)(1+u\,\eta), \quad (16)$$

where η is a random number with uniform probability density in $[-1,1]$, and u is a real number smaller than unity that

monitors the noise level, $u=0.1$. Figures 4(b)–4(d) show that the noise amplifies the errors that were visible in the non-noisy reconstruction, essentially at the edges of the grating. As a consequence, the image of the tore loses part of its homogeneity. Yet, the reconstruction remains globally satisfactory.

V. CONCLUSION

We have presented a numerical study of the resolution of an optical tomography experiment in various configurations: homogeneous space, prism, and metallic layer grating substrate, under the renormalized Born approximation. We have shown that the resolution of the image is slightly better when the objects are deposited on a prism than when they are in a vacuum. The presence of a metallic layer that supports short-range surface plasmon does not ameliorate the transverse resolution as the surface wave is only weakly excited by the objects. On the other hand, when the objects are deposited on a grating that has been optimized to excite the short-range surface plasmon of the metallic layer, one obtains a spectacular improvement of the resolution. We have also addressed the inversion issue when the renormalized Born approximation fails. We have shown that accounting for multiple scattering within the object while neglecting the coupling with the substrate is enough to improve significantly the image. This approximation simplifies and speeds up greatly the resolution of the near-field equation since we use the field susceptibility tensor of the homogeneous space. Last we have checked that our reconstruction algorithm was robust to noise.

[1] S. B. Ippolito, B. B. Goldberg, and M. S. Ünlü, Appl. Phys. Lett. **78**, 4071 (2001).

[2] M. Dyba and S. W. Hell, Phys. Rev. Lett. **88**, 163901 (2002).

[3] N. Streibl, J. Opt. Soc. Am. A **2**, 121 (1985).

[4] V. Lauer, J. Microsc. **205**, 165 (2002).

[5] P. C. Chaumet, K. Belkebir, and A. Sentenac, Phys. Rev. B **69**, 245405 (2004a).

[6] G. Cragg and P. So, Opt. Lett. **25**, 46 (2000).

[7] P. S. Carney and J. C. Schotland, J. Opt. Soc. Am. A **20**, 542 (2003).

[8] K. Belkebir, P. C. Chaumet, and A. Sentenac, J. Opt. Soc. Am. A **22**, 1889 (2005).

[9] B. Rothenhäusler and W. Knoll, Nature (London) **332**, 615 (1982).

[10] I. I. Smolyaninov, J. Elliott, A. V. Zayats, and C. C. Davis, Phys. Rev. Lett. **94**, 057401 (2005).

[11] A. Sentenac, P. C. Chaumet, and K. Belkebir, Phys. Rev. Lett. **97**, 243901 (2006).

[12] Z. Liu, S. Durant, H. Lee, Y. Pikus, N. Fang, Y. Xiong, C. Sun, and X. Zhang, Nano Lett. **7**, 403 (2007).

[13] K. Belkebir, P. C. Chaumet, and A. Sentenac, J. Opt. Soc. Am. A **23**, 586 (2006).

[14] E. Wolf, Opt. Commun. **1**, 153 (1969).

[15] R. Petit, *Electromagnetic Theory of Gratings* (Springer-Verlag, Berlin, 1980).

[16] A. L. Fehrembach, D. Maystre, and A. Sentenac, J. Opt. Soc. Am. A **19**, 1136 (2002).

[17] E. N. Economou, Phys. Rev. **182**, 539 (1969).

[18] H. Raether, *Surface Plasmons on Smooth and Rough Surfaces and on Grating* (Springer-Verlag, Berlin, 1988).

[19] E. M. Purcell and C. R. Pennypacker, Astrophys. J. **186**, 705 (1973).

[20] P. C. Chaumet, A. Rahmani, F. de Fornel, and J.-P. Dufour, Phys. Rev. B **58**, 2310 (1998).

[21] A. Rahmani, P. C. Chaumet, and F. de Fornel, Phys. Rev. A **63**, 023819 (2001).

[22] P. C. Chaumet and A. Sentenac, Phys. Rev. B **72**, 205437 (2005).

[23] P. C. Chaumet, A. Rahmani, and G. W. Bryant, Phys. Rev. B **67**, 165404 (2003).

[24] P. C. Chaumet, A. Sentenac, and A. Rahmani, Phys. Rev. E **70**, 036606 (2004).

[25] A. Rahmani, P. C. Chaumet, and G. W. Bryant, Astrophys. J. **607**, 873 (2004).

[26] J. D. Jackson, *Classical Electrodynamics*, 2nd ed. (Wiley, New York, 1975).

[27] M. Paulus, P. Gay-Balmaz, and O. J. F. Martin, Phys. Rev. E **62**, 5797 (2000).

[28] J. Lekner, *Theory of Reflection of Electromagnetic and Particle Waves* (Springer, New York, 1987).

[29] P. C. Chaumet, K. Belkebir, and A. Sentenac, Opt. Lett. **29**, 2740 (2004).

[30] J. J. Goodman and P. J. Flatau, Opt. Lett. **16**, 1198 (2002).

[31] F. Bordas, N. Louvion, S. Callard, P. C. Chaumet, and A. Rahmani, Phys. Rev. E **73**, 056601 (2006).

[32] W. H. Press, B. P. Flannery, S. A. Teukolski, and W. T. Vetterling, *Numerical recipes. The Art of Scientific Computing* (Cambridge University Press, Cambridge, England, 1986).

[33] F. Simonetti, Phys. Rev. E **73**, 036619 (2006).